Graphene oxide/Al_2O_3 membrane with efficient salt rejection for water purification

Xuebing Hu, Yun Yu, Na Lin, Shuang Ren, Xiaozhen Zhang, Yongqing Wang and Jianer Zhou

ABSTRACT

To obtain efficient salt rejection in saline solution treatment, an asymmetric graphene oxide/Al_2O_3 membrane was prepared by a spin-coating process. According to microstructure measurement, the membrane has a multilayer structure and graphene oxide has been tightly coated on the surface of the Al_2O_3 membrane interlayer homogeneously. During the treatment of different aqueous salt solutions, the permeation flux and salt rejection of the membrane were investigated. The results show the permeation flux of the membrane is about 1.254 $L \cdot m^{-2} \cdot h^{-1} \cdot bar^{-1}$ and the salt rejection of the membrane reaches 28.66%, 39.24% and 43.52% for 0.01 $mol \cdot L^{-1}$ NaCl, $Cu(NO_3)_2$ and $MgSO_4$, respectively. The mechanism of the salt rejection of the membrane has been explained in this work. All these results indicate the GO/Al_2O_3 membrane shows great potential in the desalination field.

Key words | desalination, graphene oxide, membrane, salt rejection

Xuebing Hu (corresponding author)
Na Lin
Shuang Ren
Xiaozhen Zhang
Yongqing Wang
Jianer Zhou
Key Laboratory of Inorganic Membrane,
Jingdezhen Ceramic Institute,
Jingdezhen 333001,
China
E-mail: *xuebinghu2010@gmail.com*

Xuebing Hu
Yun Yu
Key Laboratory of Inorganic Coating Materials,
Shanghai Institute of Ceramics, Chinese Academy of Science,
Shanghai 201800,
China

INTRODUCTION

The increasing scarcity of fresh water sources across the globe has urged the need to develop alternative water supplies, including seawater desalination, reuse and recycling of wastewater and storm water (Mahmoud *et al.* 2015). Desalination is one of the most important and promising methods for fresh water augmentation (Elimelech & Phillip 2011). In recent times, numerous considerable efforts have been put towards obtaining fresh water from abundantly available saline seawater. Many water treatment technologies, such as ion exchange, electrodialysis, reverse osmosis and distillation, have been investigated over the past few decades (Kheriji *et al.* 2015; Bergquist *et al.* 2016; Gabarrón *et al.* 2016; Wu *et al.* 2017). Among these technologies, the pressure-driven membrane-based desalination process has attracted lots of attention due to its advantages of excellent separation rate against salts, energy savings, and being environmentally friendly (Hegab & Zou 2015; Werber *et al.* 2016; Qin *et al.* 2017).

Recently, graphene oxide (GO), which is prepared by the chemical exfoliation of graphite using strong oxidants, has been demonstrated to be a potential membrane material in the field of water purification applications due to its distinctive structural characteristics, excellent antifouling properties, high mechanical strength and negligible thickness (You *et al.* 2016; Fathizadeh *et al.* 2017; Ma *et al.* 2017). In particular, GO contains hydroxyl and epoxy functional groups on the basal planes, in addition to carbonyl and carboxyl groups located at the sheet edges (Dreyer *et al.* 2010). These oxygen-containing functional groups maintain a relatively large intersheet distance and empty spaces between nonoxidized regions, resulting in the formation of nanochannels between GO sheets that can be used for highly selective molecular and ionic separation of the GO membrane (Han *et al.* 2015; Xu *et al.* 2017). In addition, the low production cost of GO from exfoliating graphite provides a greater competitive edge in terms of cost for scaled-up fabrication of such membranes when

doi: 10.2166/ws.2018.037

compared with other more expensive nanomaterials (Goh *et al.* 2015).

In recent years, numerous studies have adopted GO as the separation layer on the polymer or ceramic matrix in the design of filtration and desalination materials (Aba *et al.* 2015; Liu *et al.* 2015). However, studies with reference to the desalting properties of the GO membrane on the asymmetric ceramic membrane support are rarely reported.

Herein, we report the preparation of the GO top membrane on the asymmetric double-layer Al_2O_3 ceramic membrane support, and use the GO/Al_2O_3 membrane to remove salt from the different aqueous salt solutions. The results demonstrate the membrane has an efficient salt rejection toward NaCl, $Cu(NO_3)_2$ and $MgSO_4$. Our work presents a simple and low-cost method for preparing a GO/Al_2O_3 membrane. The membrane exhibits many fascinating advantages such as a high rejection of salt, simple and scalable synthesis procedure and technical readiness for scaling up membrane production. All the superior performances of the membrane could open the door to opportunities to overcome the challenges in making clean water easily available.

EXPERIMENTAL

Materials

Flake graphite powders (99.9% purity) were purchased from Qingdao Sanyuan Graphite Co., Ltd. Polyacrylic acid (Dolapix CE 64) was purchased from Zschimmer & Schwarz Co., Germany. Commercial α-Al_2O_3 powders (99.9%, average particle size of 5 μm) were purchased from Zhengzhou Baige Abrasives Co., Ltd. Nano α-Al_2O_3 powders (99.99%, average particle size of 200 nm) were purchased from Shanghai Aladdin Biochemical Technology Co., Ltd.

Synthesis of GO

The synthesis of GO has been reported in our previous works (Hu *et al.* 2013). In this work, the prepared GO was diluted with deionized water to make a homogeneous GO suspension (0.5 mg·L^{-1}) for storing.

Preparation of Al_2O_3 membrane support and interlayer

The preparation process of the Al_2O_3 membrane support can be described as follows: firstly, the Al_2O_3 powders were mixed with 1 wt% PVA solution. After sieving, the obtained powders were aged for 24 h. Secondly, 1 g aged Al_2O_3 powders were uniaxially pressed in a disk (Φ24 mm) at 10 MPa. After drying at 120 °C for 3 h, these disks were sintered at 1,500 °C for 2 h. Finally, after cleaning and drying, the support disks (porosity = 40% and thickness = 1.5 mm) with an average pore size of about 400 nm were ready for use.

The Al_2O_3 membrane interlayer was prepared by a dip-coating method. Briefly, 3 wt% PVA as a binder, 0.15 wt% Dolapix CE 64 as a dispersant and 10 wt% nano Al_2O_3 powders were mixed and stirred until the slurry dispersed homogeneously. The above-mentioned Al_2O_3 support disk was placed on the surface of the slurry for 5 s and dried at 50 °C for 3 h. Thereafter, the support with the nano Al_2O_3 layer was sintered at 1,500 °C for 2 h. Finally, the nano Al_2O_3 membrane interlayer with an average pore size of about 80 nm and a thickness of about 10 μm was obtained.

Preparation of GO membrane top layer

The GO membrane top layer was deposited on the Al_2O_3 membrane interlayer by a spin-coating process. Briefly, the GO suspension was dropped on the above-mentioned membrane interlayer and spun at 200 rpm for 5 s and 3,600 rpm for 5 s. To enhance the mechanical property of the GO membrane top layer, it was dried at 60 °C for 3 h. In order to obtain the definite thickness of the GO membrane, the process was repeated three times.

Characterization and measurement methods

The salt rejection experiments were carried out in a dead-end filtration membrane apparatus at room temperature. The transmembrane pressure (TMP) was monitored by a high-pressure nitrogen flow control valve. The TMP was kept at 4 bar during the experiment. The three different laboratory-made concentrations of aqueous NaCl, $Cu(NO_3)_2$ and $MgSO_4$ solutions used in this study were 0.01 mol·L^{-1}, 0.05 mol·L^{-1}, and 0.1 mol·L^{-1}, respectively. The conductivities

of the feed and permeate solutions were measured by a conductivity meter (DDSJ 308, Shanghai Instrument Electric Science Instrument Co. Ltd, Shanghai, China). The salt concentration of the permeate solutions was calculated according to the ionic solution conductivity curve. The permeate flux (J) and salt rejection (R) were calculated using the following equations, respectively:

$$J = \frac{W}{(A \times t \times P)} \tag{1}$$

$$R = \frac{(C_f - C_p)}{C_f} \times 100\% \tag{2}$$

where J is the permeate flux, W, A, t and P are the volume of collected permeate, the effective membrane area, the time duration of the experiments and the TMP, respectively. R is the salt rejection, C_f and C_p are the salt concentration in the feed and permeate solution, respectively. The molecular weight cut-off of the GO/Al_2O_3 membrane is 200 Da.

The pore size distribution of the membrane support and the membrane interlayer was measured with a mercury porosimeter (AutoPore IV 9500, Micromeritics, USA). X-ray diffraction (XRD, D8 ADVANCE, Bruker Corporation, Germany) was recorded on a D/max 2550 V diffractometer with Cu Kα radiation ($\lambda = 0.1542$ nm). The Fourier transform infrared spectroscopy (FTIR, Nicolet 5700, Thermo Electron Corporation, USA) spectra were recorded in the range 3,000–500 cm^{-1} using the KBr pressed pellet technique. Raman spectra were obtained using a LABRAM Raman microscope spectrometer (HR800, Jobin Yvon Horiba, France). The excitation wavelength was 514 nm, supplied by a He–Ne laser. The microstructure of the membrane sample was investigated by field emission scanning electron microscopy (FE-SEM, SU8220, Hitachi Group, Japan). The zeta potential of GO was determined using a zeta potential analyser (ZetaPALS, Brookhaven Instruments Corporation, USA).

RESULTS AND DISCUSSION

XRD pattern, FTIR and Raman spectra of GO

The XRD pattern of GO is shown in Figure 1(a). From Figure 1(a), GO has a single intensity peak at 11.2°, which is attributed to the (001) reflection of GO (Hu *et al.* 2018). This result indicates the flake graphite was fully oxidized after the modified Hummers treatment. According to the Bragg equation, the interlayer distance of GO is about 0.7 nm, which provides possible channels for water molecules to pass through it as a membrane filtration material.

The FTIR spectrum of GO is presented in Figure 1(b). From Figure 1(b), the intense peaks at 1,051, 1,168, 1,726 and 3,382 cm^{-1} are assigned to the epoxy (C-O-C), the phenol/hydroxyl (C-OH), the carbonyl (C = O) in carboxylic acid, and the hydroxyl (-OH), respectively (Konios *et al.* 2014). It reveals there are many oxygen functionalities in GO. These oxygen-containing polar groups cause GO to have an excellent hydrophilic property, which will be beneficial for water molecules to pass easily through the GO membrane channels (Han *et al.* 2015).

Figure 1(c) shows the Raman spectrum of GO. Two main peaks can be observed, and are assigned to the D

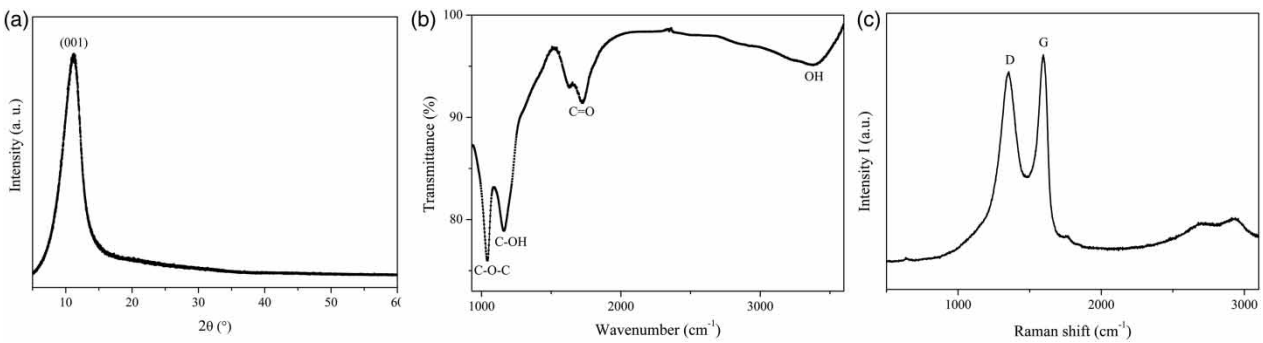

Figure 1 | (a) XRD pattern, (b) FTIR and (c) Raman spectra of GO.

and G peaks. The D peak is the fingerprint peak in graphite material with a concentration of defects. The G peak associates with the E_{2g} phonon at the Brillouin zone centre, which indicates the graphitic nature of the material (Eda & Chhowalla 2010). Figure 1(c) shows GO has a high intensity of the D peak indicating the oxidation increases the structural defects of GO. As a result, nanopores are formed in the GO.

The microstructure of the membrane

The microstructure of the GO/Al_2O_3 membrane is displayed in Figure 2. As displayed in Figure 2(a) and 2(b), it is observed that the surface of the GO membrane top layer has no obvious defects and only presents some corrugations that possibly arise from partial roll up of the edges and the random overlap of individual GO sheets (Hu *et al.* 2016).

Figure 2(c) demonstrates the finally obtained membrane can be categorized as a typical asymmetric multilayer membrane. Figure 2(c) and 2(d) display the cross-section of the membrane consisting of an Al_2O_3 membrane support, an Al_2O_3 membrane interlayer with a thickness of about 10 μm, and a GO membrane top layer with a thickness of about 800 nm. Figure 2(c) and 2(d) also show the well-layered lamellar GO membrane top layer is obtained successfully. SEM images of the membrane also verify that the GO membrane top layer has been tightly coated on the surface of the Al_2O_3 membrane interlayer, which results from the chemical interaction between hydroxyl and carboxyl groups in the interface of the GO and the Al_2O_3 membrane interlayer (Hu *et al.* 2015).

Separation performance of the membrane

To evaluate the separation performance of the GO/Al_2O_3 membrane for the treatment of different salt concentration

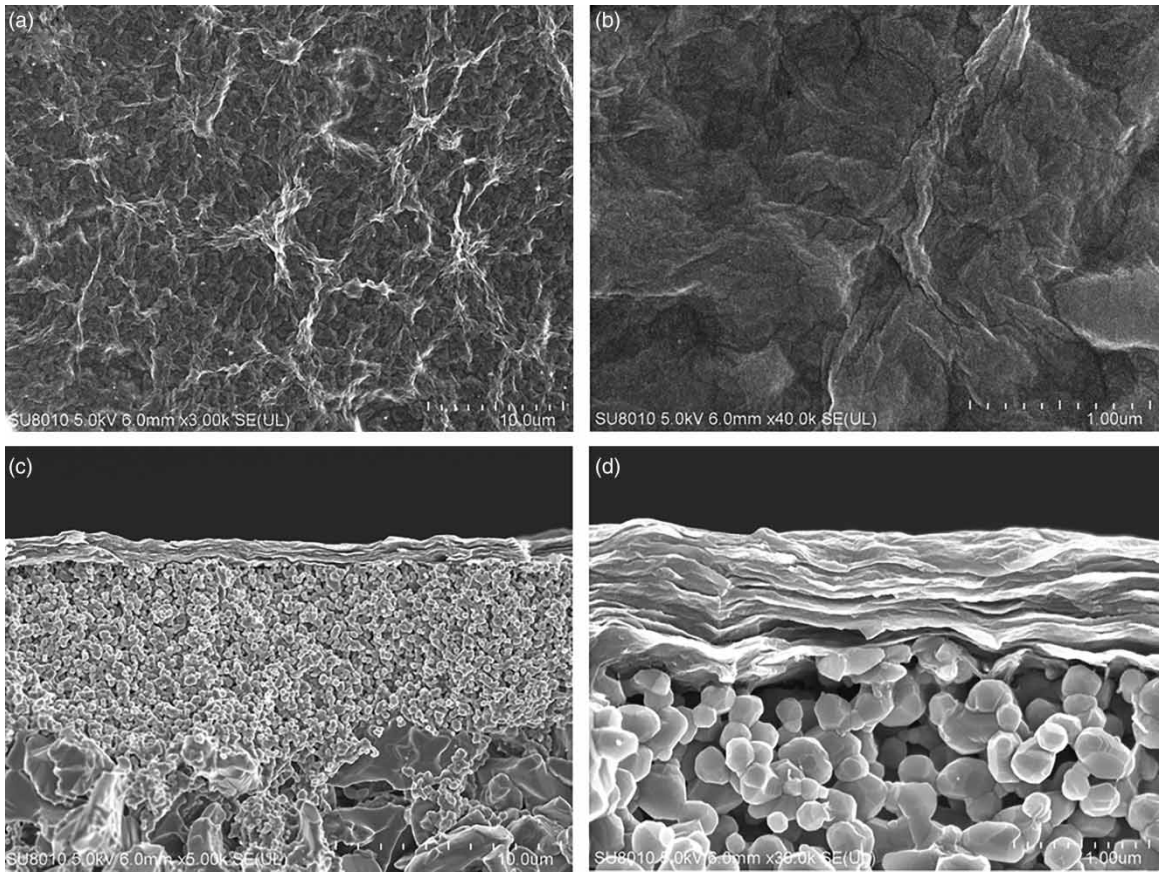

Figure 2 | SEM images of GO/Al_2O_3 membrane: various magnified surfaces (a), (b) and cross-sections (c), (d).

aqueous solutions, measurements of the permeate flux and salt rejection of the membrane were carried out. As shown in Figure 3(a), in the process of permeation, the permeate flux of the membrane almost keeps a relatively steady value (about 1.254 $L{\cdot}m^{-2}{\cdot}h^{-1}{\cdot}bar^{-1}$) for the different concentrations of aqueous NaCl, $Cu(NO_3)_2$ and $MgSO_4$ solutions, meaning that the membrane has excellent and stable filtration performance. This phenomenon should be due to the low feed concentration resulting in less membrane fouling, so that the membrane flux almost keeps constant.

The salt rejection of the membrane with varying feed is presented in Figure 3(b). From Figure 3(b), it can be found that the salt rejection increases as the salt concentration decreases for the different salt solutions, indicating the salt concentration has a great effect on the salt rejection of the membrane and the lower salt concentration is beneficial for obtaining superior salt rejection for the membrane. It is worth pointing out that at 0.01 $mol{\cdot}L^{-1}$ feed salt concentration, the salt rejection of the membrane reaches 28.66%, 39.24% and 43.52% for NaCl, $Cu(NO_3)_2$ and $MgSO_4$, respectively. Such an efficient salt rejection of the GO/Al_2O_3 membrane can be mainly explained as follows.

Initially, the salt rejection mechanism is perhaps mainly considered to be the physical sieving and Donnan effect (Wang *et al.* 2016). In general, there are many nanoscale structural defects (e.g. nanopores) that can be introduced in the basal plane of the GO sheets after the modified Hummers treatment (Dave *et al.* 2016), and these nanopores can allow for water molecules' permeation while rejecting other ions smaller in size than the nanopore. Considering the GO membrane is an assembly of GO sheets stacked together into a network of nanochannels, there are three conditions constituting the water and ion pathway in the GO membrane: nanopores, adjacent sheet edge areas and inner nanochannels (Xu *et al.* 2015). These pathways will increase the possibility of the ions passing through the membrane so that the physical sieving may have a limited effect of salt rejection in this study. As is known, the negative hydrophilic functional groups such as hydroxyl and carboxylic in GO can induce a negative charge and cause a high zeta potential on the surface of the GO membrane (Hu *et al.* 2013). The zeta potential of the GO is shown in the inset of Figure 3(b). During salt solution filtration, according to the Donnan effect, the ionic concentrations at the membrane surface are not equal to those in the bulk solution. The counter-ions concentration is higher at the membrane surface and the co-ion concentration is lower at the membrane surface compared with that of the bulk solution. When an external pressure is applied to the membrane, water can pass through the membrane, whereas co-ions are rejected due to the Donnan potential. At the same time, counter-ions are also rejected because of the requirements of electroneutrality. All these results in the GO membrane exhibit excellent rejection of salt ions.

Secondly, the membrane has a different salt rejection for NaCl, $Cu(NO_3)_2$ and $MgSO_4$ mainly due to the ion hydrated

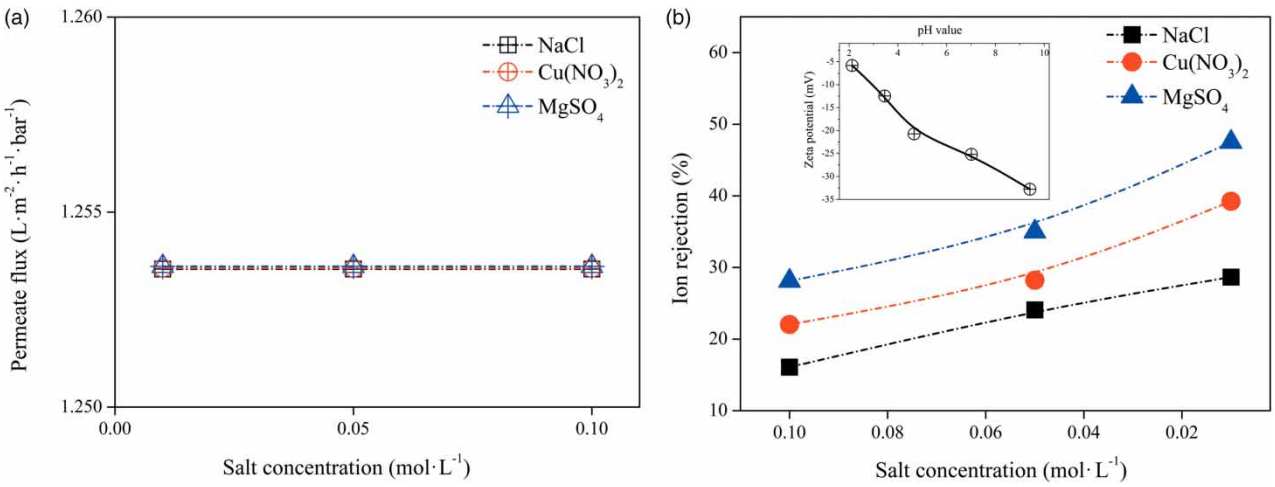

Figure 3 | (a) Time-dependent permeate flux and (b) salt rejection for the GO/Al_2O_3 membrane. The inset shows the zeta potential of GO.

radius, the ionic mobility and ion charge. The membrane has a lower salt rejection for aqueous NaCl solution since the Na^+ has a smaller hydrated radius and a higher ionic mobility compared with Cu^{2+} and Mg^{2+}, and the Cl^- has the same rule compared with NO_3^- and SO_4^{2-} (see Table 1) (Nielsen *et al.* 1990; Peeters *et al.* 1998; Zhang & Unwin 2000; Madaeni & Kazemi 2008). For the salt rejections of the aqueous $Cu(NO_3)_2$ and $MgSO_4$ solutions, although the NO_3^- has a smaller hydrated radius and a higher ionic mobility compared with SO_4^{2-}, the cation charge effect should also be considered since Mg^{2+} has a larger hydrated radius but a higher ionic mobility compared with Cu^{2+}. According to the Donnan theory, the equation for the rejection (R) of different salts as follows (Hu *et al.* 2015):

$$R = 1 - \frac{C_i^m}{C_i} = 1 - \left(\frac{|Z_i|C_i}{C_x^m + |Z_i|C_i^m}\right)^{|Z_i/Z_j|} \quad (3)$$

where C_i and C_i^m are the concentrations of co-ions in the feed and membrane, respectively, Z_i and Z_j are the valence of co-ions and counter-ions, and C_x^m is the membrane charge concentration, respectively. On the basis of Equation (3), the rejection of a 2:2 salt (such as $MgSO_4$) should be higher than for a 2:1 salt (such as $Cu(NO_3)_2$). Our result is identical to that of the theory calculation (as shown in Figure 3(b)).

Finally, the salt rejections varying with the salt concentrations may be attributed to the solution-diffusion effect (Mahlangu *et al.* 2014). Based on the classical diffusion Equation (4) as follows:

$$J = D \times \Delta C \times \frac{A_{eff}}{L_{eff}} \quad (4)$$

Table 1 | Hydrated radius and diffusion coefficient of ions

Ions	Hydrated radius/nm	Diffusion coefficient in water/10^{-9} $m^2 \cdot s^{-1}$, 25 °C
Na^+	0.365	1.33
Cu^{2+}	0.429	0.71
Mg^{2+}	0.419	0.65
Cl^-	0.332	2.03
NO_3^-	0.340	1.85
SO_4^{2-}	0.397	1.06

where J is the diffusion rate of the ions, D is the diffusion coefficient of the ions, ΔC is the concentration gradient across the membrane, A_{eff} is the effective nanochannel area of the membrane, and L_{eff} is the penetration length of ions through the membrane.

Equation (4) shows the increasing of the salt concentration will improve the diffusion rate (J) for the nanochannels present inside the GO membrane. Namely, with the increasing of the salt concentration in the feed, the rate of the salt ions' permeation through the membrane nanopores will enlarge due to the high salt concentration resulting in the strengthening salt diffusion effect, thereby leading to low salt rejection during the filtration process. The illustration for the desalination of the GO membrane top layer is shown in Figure 4. All these results demonstrate the GO/Al_2O_3 membrane would represent a next generation of the low-cost and energy-efficient membrane for ionic sieving in aqueous solution, with applications in numerous important fields.

CONCLUSION

An asymmetric GO/Al_2O_3 membrane was successfully fabricated by a spin-coating method. The microstructure

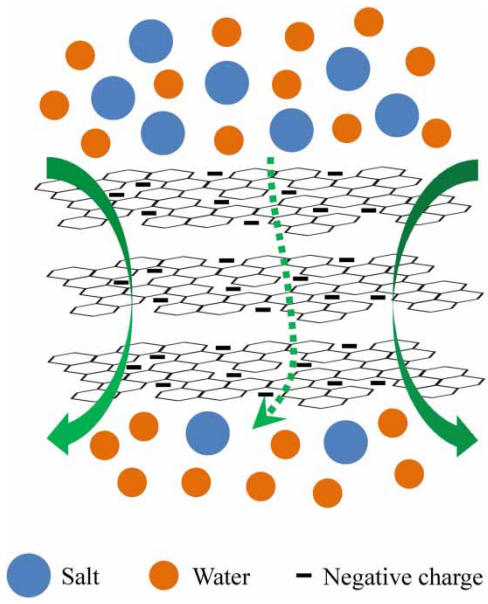

Figure 4 | Schematic of the desalination for the GO membrane top layer.

measurement shows the GO membrane top layer with a thickness of about 800 nm has been coated on the surface of the Al_2O_3 membrane interlayer homogeneously. During the treatment of different aqueous salt solutions, the membrane preserves a superior separation performance. Especially, at 0.01 mol·L^{-1} feed salt concentration, the permeate flux of the membrane keeps a relatively steady value and the salt rejection of the membrane reaches 28.66%, 39.24% and 43.52% for NaCl, $Cu(NO_3)_2$ and $MgSO_4$, respectively. The stable permeate flux and high salt rejection could ensure the GO/Al_2O_3 membrane would be a very competitive candidate for water purification.

ACKNOWLEDGEMENTS

The authors gratefully acknowledge the support of this research by the National Science Foundation of China (Grant No. 51662019) and the Foundation of Jiangxi Science and Technology Committee (Grant No. 20161ACB21008). The project also was funded by the Foundation of Jiangxi Educational Committee (Grant No. GJJ150929).

REFERENCES

Aba, N. F. D., Chong, J. Y., Wang, B., Mattevi, C. & Li, K. 2015 Graphene oxide membranes on ceramic hollow fibers – microstructural stability and nanofiltration performance. *Journal of Membrane Science* **484**, 87–94.

Bergquist, A. M., Choe, J. K., Strathmann, T. J. & Werth, C. J. 2016 Evaluation of a hybrid ion exchange-catalyst treatment technology for nitrate removal from drinking water. *Water Research* **96**, 177–187.

Dave, S. H., Gong, C., Robertson, A. W., Warner, J. H. & Grossman, J. C. 2016 Chemistry and structure of graphene oxide via direct imaging. *ACS Nano* **10** (8), 7515–7522.

Dreyer, D. R., Park, S., Bielawski, C. W. & Ruoff, R. S. 2010 The chemistry of graphene oxide. *Chemical Society Reviews* **39** (1), 228–240.

Eda, G. & Chhowalla, M. 2010 Chemically derived graphene oxide: towards large-area thin-film electronics and optoelectronics. *Advanced Materials* **22** (22), 2392–2415.

Elimelech, M. & Phillip, W. A. 2011 The future of seawater desalination: energy, technology, and the environment. *Science* **333** (6043), 712–717.

Fathizadeh, M., Xu, W. L., Zhou, F., Yoon, Y. & Yu, M. 2017 Graphene oxide: a novel 2-dimensional material in membrane separation for water purification. *Advanced Materials Interfaces* **4** (5), 1600918.

Gabarrón, S., Gernjak, W., Valero, F., Barceló, A., Petrovic, M. & Rodríguez-Roda, I. 2016 Evaluation of emerging contaminants in a drinking water treatment plant using electrodialysis reversal technology. *Journal of Hazardous Materials* **309**, 192–201.

Goh, K., Setiawan, L., Wei, L., Si, R., Fane, A. G., Wang, R. & Chen, Y. 2015 Graphene oxide as effective selective barriers on a hollow fiber membrane for water treatment process. *Journal of Membrane Science* **474**, 244–253.

Han, Y., Jiang, Y. & Gao, C. 2015 High-flux graphene oxide nanofiltration membrane intercalated by carbon nanotubes. *ACS Applied Materials & Interfaces* **7** (15), 8147–8155.

Hegab, H. M. & Zou, L. 2015 Graphene oxide-assisted membranes: fabrication and potential applications in desalination and water purification. *Journal of Membrane Science* **484**, 95–106.

Hu, X., Yu, Y., Hou, W., Zhou, J. & Song, L. 2013 Effects of particle size and pH value on the hydrophilicity of graphene oxide. *Applied Surface Science* **273**, 118–121.

Hu, X., Yu, Y., Zhou, J., Wang, Y., Liang, J., Zhang, X., Chang, Q. & Song, L. 2015 The improved oil/water separation performance of graphene oxide modified Al_2O_3 microfiltration membrane. *Journal of Membrane Science* **476**, 200–204.

Hu, X., Yu, Y., Wang, Y., Wang, Y., Zhou, J. & Song, L. 2016 Highly transparent superhydrophilic graphene oxide coating for antifogging. *Materials Letters* **182**, 372–375.

Hu, X., Yu, Y., Chen, Z., Zhang, X., Wang, Y. & Zhou, J. 2018 Efficient reduction of graphene oxide film by low temperature heat treatment and its effect on electrical conductivity. *Materials Testing* **60** (1), 102–106.

Kheriji, J., Tabassi, D. & Hamrouni, B. 2015 Removal of Cd(II) ions from aqueous solution and industrial effluent using reverse osmosis and nanofiltration membranes. *Water Science and Technology* **72** (7), 1206–1216.

Konios, D., Stylianakis, M. M., Stratakis, E. & Kymakis, E. 2014 Dispersion behaviour of graphene oxide and reduced graphene oxide. *Journal of Colloid and Interface Science* **430**, 108–112.

Liu, H., Wang, H. & Zhang, X. 2015 Facile fabrication of freestanding ultrathin reduced graphene oxide membranes for water purification. *Advanced Materials* **27** (2), 249–254.

Ma, J., Guo, X., Ying, Y., Liu, D. & Zhong, C. 2017 Composite ultrafiltration membrane tailored by MOF@GO with highly improved water purification performance. *Chemical Engineering Journal* **313**, 890–898.

Madaeni, S. S. & Kazemi, V. 2008 Treatment of saturated brine in chlor-alkali process using membranes. *Separation and Purification Technology* **61** (1), 68–74.

Mahlangu, T. O., Hoek, E. M. V., Mamba, B. B. & Verliefde, A. R. D. 2014 Influence of organic, colloidal and combined fouling on NF rejection of NaCl and carbamazepine: role of solute–foulant–membrane interactions and cake-enhanced

concentration polarisation. *Journal of Membrane Science* **471**, 35–46.

Mahmoud, K. A., Mansoor, B., Mansour, A. & Khraisheh, M. 2015 Functional graphene nanosheets: the next generation membranes for water desalination. *Desalination* **356**, 208–225.

Nielsen, L. P., Christensen, P. B., Revsbech, N. P. & Sørensen, J. 1990 Denitrification and oxygen respiration in biofilms studied with a microsensor for nitrous oxide and oxygen. *Microbial Ecology* **19** (1), 63–72.

Peeters, J. M. M., Boom, J. P., Mulder, M. H. V. & Strathmann, H. 1998 Retention measurements of nanofiltration membranes with electrolyte solutions. *Journal of Membrane Science* **145** (2), 199–209.

Qin, Y., Hu, Y., Koehler, S., Cai, L., Wen, J., Tan, X., Xu, W. L., Sheng, Q., Hou, X., Xue, J., Yu, M. & Weitz, D. 2017 Ultrafast nanofiltration through large-area single-layered graphene membranes. *ACS Applied Materials & Interfaces* **9** (11), 9239–9244.

Wang, J., Zhang, P., Liang, B., Liu, Y., Xu, T., Wang, L., Cao, B. & Pan, K. 2016 Graphene oxide as an effective barrier on a porous nanofibrous membrane for water treatment. *ACS Applied Materials & Interfaces* **8** (9), 6211–6218.

Werber, J. R., Osuji, C. O. & Elimelech, M. 2016 Materials for next-generation desalination and water purification membranes. *Nature Reviews Materials* **1**, 16018.

Wu, C. Y., Chen, S. S., Zhang, D. Z. & Kobayashi, J. 2017 Hg removal and the effects of coexisting metals in forward osmosis and membrane distillation. *Water Science and Technology* **75** (11), 2622–2630.

Xu, Q., Xu, H., Chen, J., Lv, Y., Dong, C. & Sreeprasad, T. S. 2015 Graphene and graphene oxide: advanced membranes for gas separation and water purification. *Inorganic Chemistry Frontiers* **2** (5), 417–424.

Xu, W. L., Fang, C., Zhou, F., Song, Z., Liu, Q., Qiao, R. & Yu, M. 2017 Self-assembly: a facile way of forming ultrathin, high-performance graphene oxide membranes for water purification. *Nano Letters* **17** (5), 2928–2933.

You, Y., Sahajwalla, V., Yoshimura, M. & Joshi, R. K. 2016 Graphene and graphene oxide for desalination. *Nanoscale* **8** (1), 117–119.

Zhang, J. & Unwin, P. R. 2000 Microelectrochemical measurements at expanding droplets (MEMED): investigation of cupric ion stripping kinetics in a two-phase oil/water system. *Physical Chemistry Chemical Physics* **2** (6), 1267–1271.

First received 11 November 2017; accepted in revised form 31 January 2018. Available online 15 February 2018